Midwave infrared quantum dot avalanche photodiode

David A. Ramirez,[a] Jiayi Shao, Majeed M. Hayat, and Sanjay Krishna[b]
Department of Electrical and Computer Engineering and the Center for High Technology Materials (CHTM), University of New Mexico (UNM), 1313 Goddard St. SE, Albuquerque, New Mexico 87106, USA

(Received 15 July 2010; accepted 5 November 2010; published online 1 December 2010)

We report the first demonstration of a GaAs based avalanche photodiode (APD) operating in the midwave infrared region (3–5 μm). In the device, called the quantum dot avalanche photodiode, an intersubband quantum dots-in-a-well detector is coupled with an APD through a tunnel barrier. Using this approach, we have increased the photocurrent and reached a conversion efficiency of 12%, which is one of the highest reported conversion efficiencies for any quantum dot detector.
© *2010 American Institute of Physics*. [doi:10.1063/1.3520519]

Single-photon detectors represent the ultimate device in terms of their sensitivity, and they are widely used in a variety of low light level applications. Single-photon avalanche photodiodes (SPADs) are obtained by operating avalanche photodiodes (APDs) close to the breakdown bias threshold, in what is called as the Geiger mode.[1] However, present day APDs are limited to wavelengths below 2 μm. In this paper, we report the first demonstration of a GaAs based APD operating in the midwave infrared region (MWIR) (3–5 μm). In the quantum dot avalanche photodiode (QDAP),[2] intersubband absorption in the quantum confined dots-in-a-well (DWELL) heterostructure is exploited for MWIR detection, and multiplication in the APD is engineered to obtain a large conversion efficiency (CE). The conversion efficiency η_{conv} is the product of the internal quantum efficiency η and the photoconductive gain g and is given by $\eta_{\text{conv}}=\eta g =R(h\nu)/q$, where R is the responsivity, q is the charge of the electron, and $h\nu$ is the photoexcitation energy. Using this approach, we have increased the photocurrent by a factor of 14 and reached a CE of 12%, which is one of the highest reported CEs for any quantum dot detector.

Various approaches have been explored to realize single-photon detectors. They include superconducting detectors, photomultiplier tubes (PMTs), and APDs. While superconducting detectors offer the highest quantum efficiency and the lowest dark count rate, they are limited to very low operating temperature (<10 K). PMTs have demonstrated very good performance in the visible region but are very bulky and are not compatible with the standard semiconductor manufacturing processes. PMTs also require very high voltages and are sensitive to magnetic fields. APDs represent the most promising scalable technology as they are based on semiconductors, such as Si, GaAs, and InP, and can be made into large format arrays. APDs can be operated in two modes. In the linear mode, the APD is biased below breakdown and the output photocurrent is "amplified" through the avalanche of impact ionizations. In the Geiger or single-photon avalanche detector mode, the APD is biased just below the breakdown voltage and a gated pulse is used to drive it above breakdown for a short duration. An incoming photon during this gated pulse triggers a cascade, or avalanche, of impact ionization events leading to a large current. Various active and passive quenching circuits have been developed to limit the current flowing in the APD and to reset it for the next pulse.[3] However, all GaAs based SPADs available today are limited to wavelengths less than 2 μm.[4] Hamamatsu has an extended InGaAs APD that operates up to 1.7 μm.[4]

In the quantum dot avalanche photodiode, an intersubband quantum dots-in-a-well detector is coupled with an APD through a tunnel barrier [see Fig. 1(a)]. The photon absorption and generation of carriers take place in the DWELL section while the avalanche section provides internal gain. The demonstration of the linear mode operation of the QDAP signifies a major achievement as it opens up the possibility of obtaining SPADs in the midwave infrared range. This would have a dramatic impact on many applications that require high-sensitivity MWIR detectors, including astronomy and biomedical diagnostics.

The operating principle of the QDAP is shown in Fig. 1. Operationally, the QDAP can be divided into two stages: (a) the photogeneration of carriers and (b) the avalanche multiplication of the photogenerated carriers. The absorption of photons and photogeneration of electrons are due to intersubband transitions in the quantum dots (QDs). Among the various QD heterostructures, the DWELL detector is among the most promising alternatives for terrestrial applications.[5] The DWELL heterostructure is a hybrid between a conventional quantum well infrared photodetector (QWIP) and a quantum dot infrared photodetector (QDIP) and draws from the advantages of both of these technologies. DWELL detectors operate under normal incidence conditions with low dark current like the QDIP and have good operating wavelength control like the QWIP. In addition, DWELL detectors benefit from a mature growth and processing technology of III-V semiconductors, making it possible to produce devices with good spatial uniformity over a large area. This characteristic is essential for fabricating large format focal plane arrays (FPAs). Recently, Ting *et al.*[6] demonstrated a 1 megapixel DWELL FPA with peak response at 8.5 μm.

Thus, the spectral response of the QDAP is determined by the DWELL section. On the other hand, the avalanche multiplication, resulting from the injection of the photogenerated electrons into the avalanche region, takes place in the APD section. To control the individual responses of the DWELL and the APD sections, the voltage applied between the top and middle contacts and the voltage between the middle and bottom contacts are independently varied. Figure

[a]Electronic mail: davramir@unm.edu.
[b]Electronic mail: skrishna@chtm.unm.edu.

 © 2010 American Institute of Physics

Author complimentary copy. Redistribution subject to AIP license or copyright, see http://apl.aip.org/apl/copyright.jsp

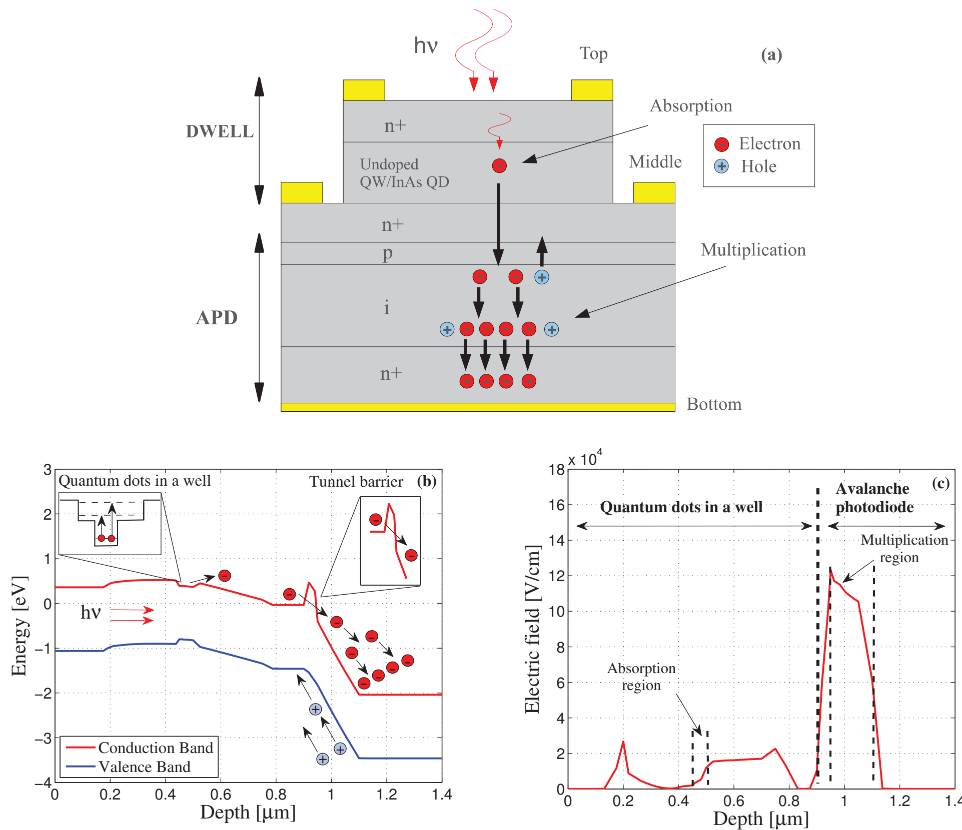

FIG. 1. (Color online) Structure and principle of operation. (a) Heterostructure schematic of the QDAP showing the separate absorption and multiplication regions. (b) Calculated band diagram of the QDAP using SENTAURUS simulation tool with the absorption and multiplication sections reverse biased at voltages of 0.5 and 2.0 V, respectively. (c) Theoretical simulation of the electric field profile in the device, confirming that the maximum electric field is dropped across the multiplication region.

1(a) shows the heterostructure of the QDAP and illustrates the absorption and multiplication stages. When the incident radiation of energy $h\nu$, where h is the Planck's constant and ν is the frequency of the incident radiation, is shone on the device, the incident photons are absorbed in the active region of the DWELL section. As a result, the electrons in the ground state of the quantum dots are promoted to a set of bound states within the quantum well. Once these electrons are extracted from the quantum well, they drift, as a result of the applied electric field, toward the APD section of the device. This is illustrated in Fig. 1(b). To reach the avalanche region located in the APD section, the electrons need to tunnel through the barrier established by the *p*-type layer, as shown in Fig. 1(b). In the high-field avalanche region, the injected electrons experience a series of impact ionizations that multiply them. Finally, the multiplied electrons are collected at the bottom contact. For these processes to take place, the external biasing circuit used to operate the QDAP has to be designed in such a way that the flow of electrons is from the top to the bottom contact. This mode of operation is achieved when both sections of the QDAP are reverse biased, i.e., $V_{top} < V_{mid} < V_{bot}$. A customized biasing circuit was built to enable this configuration. Figure 1(c) shows the theoretically calculated electric field in the QDAP, indicating that most of the applied field drops across the APD.

The n-i-n DWELL detector was grown on top of the p-i-n APD section using solid source molecular beam epitaxy. The DWELL section of the QDAP consists of the structure reported by Shenoi *et al.*[7] This heterostructure design incorporated a lower strain per stack, leading to a large number of stacks (30) compared to the previous designs.[8] The DWELL consists of *n*-doped InAs dots in an $In_{0.15}Ga_{0.85}As/GaAs$ well and $Al_{0.10}Ga_{0.90}As$ as the barrier. These layers are sandwiched between two highly doped *n*-GaAs layers. The APD was a standard p-i-n diode with a GaAs multiplication region of 0.15 μm. The multiplication region was made thin to achieve a small avalanche breakdown voltage and to enhance the dead-space effect.[9] It is known that in thin multiplication regions, the dead-space reduces the multiplication noise, also called the excess noise, introduced by the avalanche multiplication process in APDs.[9,10] The multiplication noise is a result of the stochastic nature of the impact ionization process.

To demonstrate the operation of the QDAP, a series of radiometric measurements were carried out. First, the spectral response of the QDAP was measured using a Thermo Nicolet Fourier transform infrared spectrometer. Figure 2(a) shows the measured conversion efficiency of the DWELL section as a function of wavelength for a reverse bias of 2 V across the DWELL. It can be seen that the conversion efficiency peaks at 5 μm. The next step was to demonstrate the ability to separately control the absorption and the multiplication response of the QDAP. To this end, the photocurrent of the QDAP detectors was measured with the devices cooled down to liquid nitrogen temperature (77 K). To create carriers in the DWELL section, the devices were irradiated using a 3.39 μm laser beam chopped at a frequency of 400 Hz. A specially designed circuit board was used to bias the devices and amplify the photocurrent. Then, the amplified signal was fed into an SR770 fast Fourier transform network analyzer. In the first experiment, the photocurrent in the QDAP was plotted as a function of the bias across the DWELL section [shown in Fig. 2(b)]. The current increases linearly with the applied bias as expected. The inset in Fig. 2(b) shows the structure of the device under test. In the second experiment, the photoelectron generation in the DWELL section was fixed by keeping the DWELL section biased at a fixed value (0.5 V). The multiplication gain of the APD was

Author complimentary copy. Redistribution subject to AIP license or copyright, see http://apl.aip.org/apl/copyright.jsp

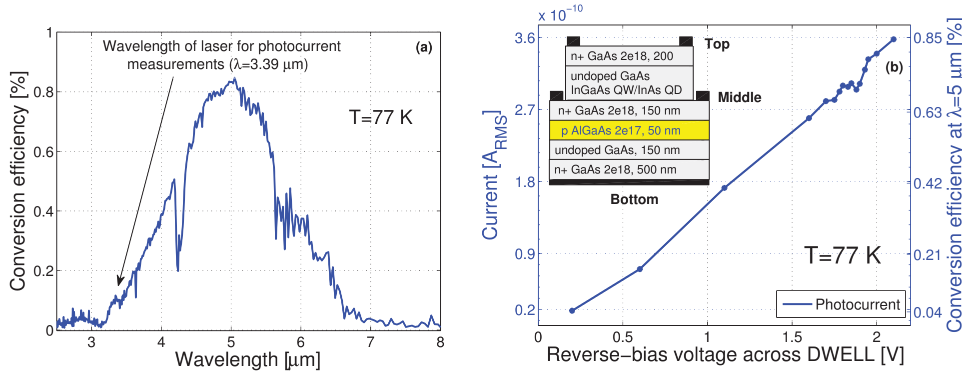

FIG. 2. (Color online) Conversion efficiency. (a) Conversion efficiency of the DWELL absorber as a function of wavelength for an applied bias of 2 V. (b) Photocurrent and conversion efficiency of the DWELL section at $\lambda = 5$ μm as a function of the reverse bias. The inset illustrates the structure of the device under text.

then varied by changing the voltage across the APD. Figure 3 shows the photocurrent and the total multiplied noise of the heterojunction QDAP structure as a function of the reverse bias across the APD for a fixed reverse bias of 0.5 V across the DWELL section. It can be seen that for a fixed voltage across the DWELL section, as the reverse bias across the APD increases, the photocurrent of the device increases in a fashion dictated by the multiplication gain of the APD. In addition, compared to the photocurrent characteristics of the DWELL section alone, the QDAP photocurrent is distinctly different. Our measurements demonstrate that the response of the DWELL and APD sections of the device can be controlled independently, and the overall response of the QDAP can be enhanced. In addition, we have found that the signal-to-noise ratio (SNR) of the QDAP (results not shown) increases as a function of the reverse bias voltage. However, after reaching a maximum value, the SNR decreases as a result of the faster increase of the noise. The SNR starts to decrease at a reverse bias voltage across the APD of about 1.9 V, which corresponds to a multiplication gain close to 6. The inset in Fig. 3 shows the calculated excess noise factor of the device (dots) and the excess noise factor predicted by

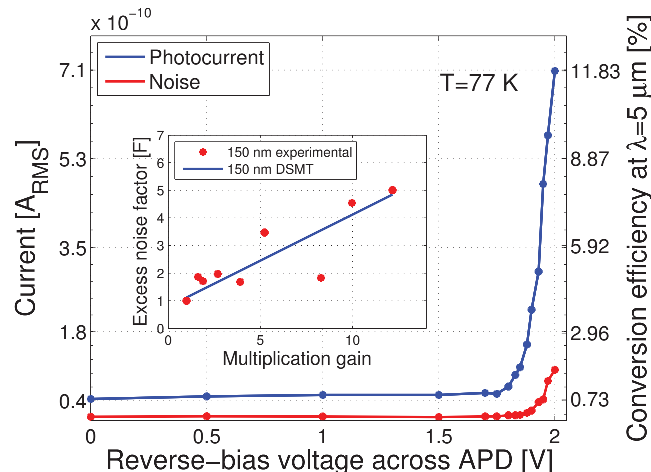

FIG. 3. (Color online) Photocurrent, conversion efficiency, and noise of the QDAP as functions of the reverse bias voltage across the APD section for a fixed applied bias of 0.5 V across the DWELL section. The inset shows the calculated excess noise factor of the device (dots) and the excess noise factor predicted by the dead-space multiplication theory (DSMT) (solid curve). Note that if the DWELL absorber was operated at 2 V [as in Fig. 2(a)], the peak CE at $\lambda = 5$ μm would be about 12%, which is one of the highest reported CE for any QD based midinfrared detector.

the dead-space multiplication theory[11,12] (DSMT) (solid curve) as a function of the multiplication gain. The excess noise factor was estimated by fitting the measured data to the excess noise factor of a GaAs multiplication region of 150 nm predicted by the DSMT. It has been previously shown[12] that the DSMT accurately predicts the excess noise factor of thin III-V avalanche photodiodes. It can be seen that with the exception of the excess noise factor for a multiplication gain of ~8.2, the calculated excess noise factor closely follows the trend predicted by the DSMT.

To compare the performance of the QDAP with that of the DWELL, their conversion efficiencies η_{conv} were measured. The conversion efficiency in the DWELL was increased by a factor of 14 due to the gain introduced by the avalanche multiplication stage of the QDAP. From Fig. 2(a), we see that at $\lambda = 5$ μm, the peak conversion efficiency of the DWELL alone is measured to be 0.84% at a reverse bias of 2.0 V. Therefore, by operating the QDAP with the DWELL section reverse biased at 2.0 V, it is possible to obtain a maximum conversion efficiency of about 12%.

This work was supported by the AFRL, under Grant No. FA9453-07-C-0171, and by the National Science Foundation, under Award Nos. ECS-0601645 and ECS-0428756.

[1] S. Cova, M. Ghioni, A. Lotito, I. Rech, and F. Zappa, J. Mod. Opt. **51**, 1267 (2004).
[2] S. Krishna, O. H. Kwon, and M. M. Hayat, IEEE J. Quantum Electron. **41**, 1468 (2005).
[3] S. Cova, M. Ghioni, A. Lacaita, C. Samori, and F. Zappa, Appl. Opt. **35**, 1956 (1996).
[4] InGaAs APD: G8931-20, Hamamatsu datasheet, pp. 1–2, 2009.
[5] A. V. Barve, S. J. Lee, S. K. Noh, and S. Krishna, Laser Photonics Rev. 1-13 (2009).
[6] D. Z.-Y. Ting, S. V. Bandara, S. D. Gunapala, J. M. Mumolo, S. A. Keo, C. J. Hill, J. K. Liu, E. R. Blazejewski, Sir B. Rafol, and Y.-C. Chang, Appl. Phys. Lett. **94**, 111107 (2009).
[7] R. V. Shenoi, R. S. Attaluri, A. Siroya, J. Shao, Y. D. Sharma, A. Stintz, T. E. Vandervelde, and S. Krishna, J. Vac. Sci. Technol. B **26**, 1136 (2008).
[8] R. S. Attaluri, S. Annamali, K. T. Posani, A. Stintz, and S. Krishna, J. Vac. Sci. Technol. B **24**, 1553 (2006).
[9] M. M. Hayat, O.-H. Kwon, S. Wang, J. C. Campbell, B. E. A. Saleh, and M. C. Teich, IEEE Trans. Electron Devices **49**, 2114 (2002).
[10] P. Yuan, S. Wang, X. Sun, X. G. Zheng, A. L. Holmes, Jr., and J. C. Campbell, IEEE Photonics Technol. Lett. **12**, 1370 (2000).
[11] M. M. Hayat, B. E. A. Saleh, and M. C. Teich, IEEE Trans. Electron Devices **39**, 546 (1992).
[12] M. A. Saleh, M. M. Hayat, P. P. Sotirelis, A. L. Holmes, J. C. Campbell, B. E. A. Saleh, and M. C. Teich, IEEE Trans. Electron Devices **48**, 2722 (2001).

Author complimentary copy. Redistribution subject to AIP license or copyright, see http://apl.aip.org/apl/copyright.jsp